Journal of Hydraulic Research

ISSN: 0022-1686 (Print) 1814-2079 (Online) Journal homepage: http://www.tandfonline.com/loi/tjhr20

Parameterizing suspended canopy effects in a three-dimensional hydrodynamic model

Fearghal O'Donncha, Michael Hartnett & David R. Plew

To cite this article: Fearghal O'Donncha, Michael Hartnett & David R. Plew (2015): Parameterizing suspended canopy effects in a three-dimensional hydrodynamic model, Journal of Hydraulic Research, DOI: 10.1080/00221686.2015.1093036

To link to this article: http://dx.doi.org/10.1080/00221686.2015.1093036

Journal of Hydraulic Research, 2015
http://dx.doi.org/10.1080/00221686.2015.1093036

Research paper

Parameterizing suspended canopy effects in a three-dimensional hydrodynamic model

FEARGHAL O'DONNCHA, Research Scientist, *IBM Research – Ireland, Damastown Ind. Park, Mulhuddart, Dublin 15, Ireland*
Email: feardonn@ie.ibm.com (author for correspondence)

MICHAEL HARTNETT, Professor, *Department of Civil Engineering, National University of Ireland, Galway, Ireland*
Email: michael.hartnett@nuigalway.ie

DAVID R. PLEW, Scientist, *Hydrodynamics Group, National Institute of Water and Atmospheric Research (NIWA), PO Box 8602, Christchurch, New Zealand*
Email: david.plew@niwa.co.nz

ABSTRACT
This paper presents an amendment of an existing three-dimensional hydro-environmental model (Environmental Fluid Dynamics Code) to incorporate effects of suspended canopies on the vertical flow structure. Five different modelling approaches are investigated, encompassing hydrodynamic form drag imparted by the suspended canopy, an amended two-equation turbulence scheme representing turbulence generated locally by elements within the canopy, and three separate formulations for vertical profiles of drag coefficients. Data from laboratory experiments with rigid cylinders are used to validate the calculations of velocity and shear stresses. The results show that the most accurate reproduction of the canopy flow was obtained using a vertically varying drag coefficient along with a two-equation turbulence closure scheme that includes additional turbulence production and dissipation terms. The numerical model reproduced velocity profiles accurately, but the shear stresses are slightly overestimated.

Keywords: Canopy flow; hydrodynamics; numerical modelling; turbulence

1 Introduction

Aquatic canopies can significantly impact the natural ecosystem by altering hydrodynamic conditions, which in turn can modify transport rates of sediment, nutrients, contaminants and dissolved oxygen in aquatic systems (Ghisalberti & Nepf, 2002). A large body of research exists concerning the effects of bottom-growing, submerged or emergent canopies on flows (Nepf & Vivoni, 2000). Another form of canopy is the suspended type, which differs in that it extends downwards from the free surface, with a gap between the canopy and the bed (Fig. 1). Common examples of suspended canopies include cages, rafts and longlines used in aquaculture and even marine hydrokinetic turbines deployed from surface-moored infrastructure (King & Tryfonas, 2009). Field studies have demonstrated that suspended canopies alter ambient flows in a number of ways such as amended current speeds and directions within and below the canopy (Blanco, Zapata, & Morono, 1994; Plew, Stevens, Spigel, & Hartstein, 2005). These hydrodynamic modifications have important implications for a range of industries. For aquaculture farms, flow speeds directly affect the growth and feeding rates of marine bivalves by governing the supply of nutrients to the organisms (Lenihan, Peterson, & Allen, 1996). The production capacity of marine energy devices can be reduced considerably by the flow attenuation induced by the installations themselves and the supporting infrastructure (Shapiro, 2010). Resulting flow acceleration beneath the canopy can also cause ecosystem changes through, for example, increased bed shear stresses (Neill, Litt, Couch, & Davies, 2009), and modified sediment deposition and resuspension patterns (Hartstein & Stevens, 2005). Thus, understanding the hydro-environmental effects of suspended canopies is important for predicting, among others things, aquaculture carrying capacity, efficiency of marine energy devices, and environmental impacts.

While differences exist between a suspended canopy and those that are submerged or emergent, some effects are comparable (Plew, 2011a). Studies of submerged vegetated canopies

Received 19 March 2014; accepted 8 September 2015/Currently open for discussion.

ISSN 0022-1686 print/ISSN 1814-2079 online
http://www.tandfonline.com

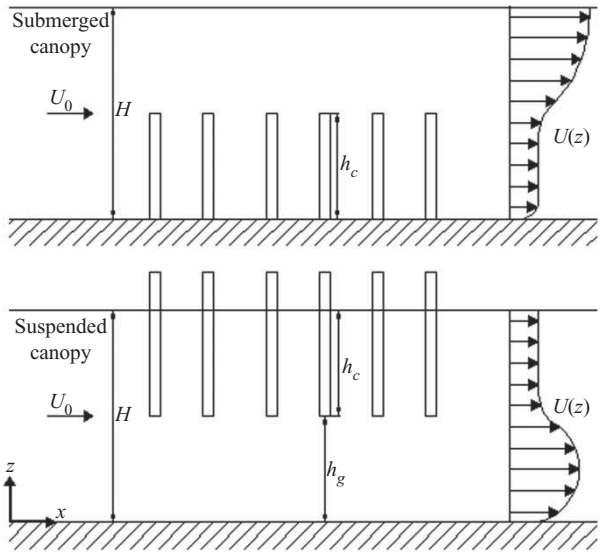

Figure 1 Schematics for both the submerged and suspended canopy configurations and associated flow profiles. H is the water depth; h_g the gap beneath the canopy; h_c the height of the canopy; and U_0 the depth-averaged velocity

have revealed a number of features relevant to suspended canopies, namely: the development of strong shear flows at the canopy interface; additional turbulence dynamics at the scale of the canopy; and a mixing layer developing at the interface of the canopy dominating vertical mixing and transport into and out of the canopy (Raupach & Thom, 1981). Nepf and Vivoni (2000) divided a submerged canopy into two regions in the vertical. In the lower canopy region, mixing and transfer with surrounding water is predominantly through longitudinal advection. In the upper canopy, exchange with the overlying water is dynamically significant to the momentum balance, and turbulence produced by shear at the top of the canopy is important. Ghisalberti and Nepf (2005) observed this to have significant implications for vertical transfer of momentum and mixing between the canopy and the overlying waters.

A number of numerical investigations of submerged canopy effects have been conducted. Naot, Nezu, and Nakagawa (1996) quantified the hydrodynamic behaviour of vegetated open channel flow using a statistical model embedded in an algebraic stress model that incorporated specific turbulence production descriptors. Other authors have adopted modified two-equation turbulence models to represent submerged canopy effects by introducing drag-related sink terms into the momentum and turbulence equations (Lopez & Garcia, 2001; Neary, 2003; Shimizu & Tsujimoto, 1994). The additional sink terms introduced two associated weighting coefficients into the turbulence equations with the published values of these coefficients varying by about 500% (Wilson, Stoesser, & Bates, 2005). King, Tinoco, and Cowen (2012) extended this modelling effort further by incorporating the effects of the canopy-member stem diameter into an amended k-ε turbulence model. However, the amended model introduced an additional five calibration parameters into the modelling process. Conversely, to reduce the calibration effort, Fischer-Antze, Stoesser, Bates, and Olsen (2001) developed a similar drag-based approach but only introduced sink terms into the momentum equation and made no modification to the k-ε turbulence model. Adopting a similar philosophy, Gao, Falconer, and Lin (2011) used a simpler, mixing length turbulence model that required fewer calibration coefficients and less computational cost than the two-equation turbulence models. These studies illustrate the many issues demanding consideration when conducting numerical studies of flow through submerged canopies.

A common feature of field studies investigating suspended canopy effects is the difficulty in accurately measuring and decomposing canopy effects based on *in situ* measurements alone. Ideally, field measurements with and without the physical impediment in place describe the impacts. However, opportunities to collect such measurements are limited. In this context, numerical modelling studies are useful in assessing the effects and implications of suspended canopy installations. This is particularly true of three-dimensional models that simulate both horizontal and vertical flow processes. However, numerical modelling studies that consider the hydrodynamic effects of suspended canopies are relatively few (McKindsey, Thetmeyer, Landry, & Silvert, 2006) with many of these studies using depth-averaged models. The effects of suspended canopies on currents have been included by either increasing bottom friction in the vicinity of farms (Grant & Bacher, 2001; Plew, 2011a) or adding an additional body force term (O'Donncha, Hartnett, & Nash, 2012; Venayagamoorthy, Fringer, Koseff, Chiu, & Naylor, 2011). In a depth-averaged model, these approaches are functionally equivalent. Effects on the vertical flow structure are either neglected or parameterized through an amended friction term (Plew, 2011b). The alternative approach is to use a more computationally expensive three-dimensional model (Shi et al., 2011).

The purpose of this study is to investigate methods of parameterizing suspended canopy effects in a three-dimensional hydrodynamic model. A hydrodynamic model was amended to simulate canopy flows extending over a specified region of the water column, with free-stream flow developing beneath. A two-equation turbulence closure model was considered, with the widely-used Mellor-Yamada approach further refined to describe canopy-effects on the intensity and length-scales of turbulence. The model was calibrated by comparison with experimental data collected from laboratory measurements of flow through a suspended canopy. The methodologies adopted to simulate suspended canopy flow processes can be broadly decomposed into two areas: a bluff-body drag force simulating the resistance exerted by the canopy, and an amended turbulence scheme describing the effects on computed turbulent stresses. The paper investigates five different modelling approaches: a constant drag term, a constant drag term with an amended turbulence scheme, and three different vertically varying drag terms with an amended turbulence scheme. In the following sections of this manuscript, the experimental data are briefly discussed,

the model output is compared against experimental data, and finally recommendations are made for further studies.

2 Methodology

Data for validating the numerical model were taken from laboratory experiments described by Plew (2011a), with a brief description given in Section 2.1. Section 2.2 presents an overview of the Environmental Fluid Dynamics Code (EFDC), while subsequent sections describe extensions to the model to parameterize canopy effects.

2.1 *Experimental data*

Full details of the experimental configuration and data analysis are presented by Plew (2011a), but a summary is provided here. Results from four experimental runs (here termed A1–A4, but referred to as B12–B15 by Plew (2011a) provide data for evaluating results from the amended models. These experimental runs were conducted under steady flow conditions in a 6 m long by 0.6 m wide flume. A suspended canopy composed of homogeneous arrays of 9.54 mm diameter aluminium cylinders extended across the full width, and the test-section length of the experimental flume. Cylinders were arranged in rows with longitudinal spacing of L_x between rows and transverse spacing L_y between cylinders. Table 1 details the experimental set-up and dimensional configurations for each run. Figure 1 is a diagram of the suspended canopy laboratory set-up, along with an associated idealized velocity profile.

Velocity measurements were collected by particle tracking velocimetry (PTV) in two vertical (x–z) planes across the flume; first, mid-way between cylinders, and then, in line with the cylinders. Velocity and turbulence values measured at each grid point were averaged horizontally in the x-direction over the distance between cylinder rows to give averaged vertical profiles for each plane. Profiles from each plane were also averaged to generate vertical profiles of spatially averaged velocity and turbulence statistics.

2.2 *Model description*

The EFDC model was used for this study – a three-dimensional, transient model that has four fully coupled major modules: hydrodynamics, sediment transport, water quality and eutrophication, and toxic chemicals fate and transport submodels. The EFDC hydrodynamic model itself comprises six transport modules, namely: dynamics, dye, temperature, salinity, near-field plume, and drifter. EFDC was originally developed at the Virginia Institute of Marine Science (Gloucester Point, VA, USA) with primary funding by the US Environmental Protection Agency and is currently supported by Tetra Tech, Inc.

EFDC is based on the three-dimensional, vertically hydrostatic, free-surface, Reynolds averaged Navier-Stokes (RANS) equations (Ji, 2008). Dynamically coupled transport equations for turbulent kinetic energy, turbulent length scale, salinity, dye and temperature are also solved. The two turbulence parameter transport equations implement the Mellor-Yamada level 2.5 turbulence closure scheme (Galperin, Kantha, Hassid, & Rosati, 1988; Mellor & Yamada, 1974). The two-equation turbulence models rely on a local time-varying eddy viscosity ν_v that parameterizes turbulent shear stress in terms of mean flow quantities (vertical shear) as:

$$-\overline{u'w'} = \nu_v \frac{\partial \bar{u}}{\partial z}; \quad -\overline{u'w'} = \nu_v \frac{\partial \bar{v}}{\partial z} \tag{1}$$

The product terms on the left hand side, $\overline{u'w'}$ and $\overline{v'w'}$, where the overbar denotes time-averaging, represent correlation between the fluctuating components of velocity, which describe the transport of momentum by turbulent motion. The standard Reynolds decomposition has been used with $u = \bar{u} + u'$; $v = \bar{v} + v'$; and $w = \bar{w} + w'$; where u, v, and w are instantaneous velocity components in the x, y, and vertical z directions, respectively; $\bar{u}$, $\bar{v}$, and $\bar{w}$ are resolvable time-averaged velocity components; and u', v', and w' are velocity fluctuations about the mean velocities. This decomposition of the instantaneous velocities into mean and fluctuating components permits modelling of the mean component at a computationally feasible resolution while the fluctuating component is parameterized within the turbulence model (Rodi, 1993).

To provide uniform resolution in the vertical direction and a free surface permitting long wave motion, a terrain-following sigma coordinate system is used (Phillips, 1957). The sigma coordinate system is a bottom-following coordinate system that maps the vertical coordinates from $-H < z^* < \eta$ to $-1 < z$

Table 1 Summary of experiments conducted to investigate suspended canopy effect on flows

	H (m)	h_g (m)	h_c (m)	L_x (m)	L_y (m)	a (m^{-1})	Q (L/s)	U_0 (ms^{-1})	C_D (−)
A1	200	100	100	150	50	1.272	10.1	0.084	1.01
A2	200	100	100	200	50	0.954	10.1	0.084	1.07
A3	200	100	100	200	100	0.477	10.3	0.086	0.85
A4	200	100	100	100	50	1.908	10.5	0.087	0.63

H is the water depth, h_g is the gap between the canopy and the bed, h_c is the height of the canopy, L_x and L_y are the streamwise and cross-stream spacing between cylinders, a is projected area per unit volume inside the canopy, Q is flow rate, U_0 is ambient upstream flow velocity and C_D is cylinder drag coefficient averaged over canopy height. Reproduced from Plew (2011a).

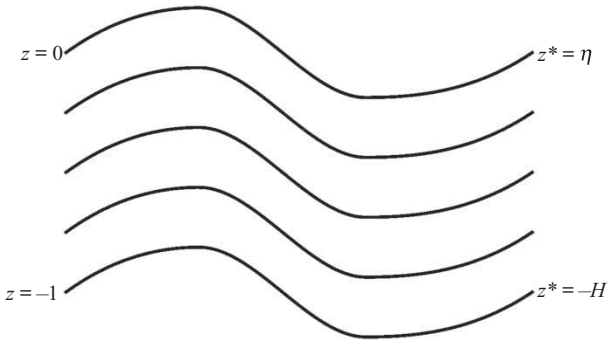

Figure 2 Sigma coordinates

< 0 with:

$$z = \frac{z^* - \eta}{H + \eta} \tag{2}$$

where the bottom is defined by $z^* = -H(x,y)$ and the water surface is defined by $z^* = -\eta(x,y,t)$ as shown in Fig. 2.

2.3 *Suspended canopy flow models*

To model canopy effects on flow dynamics, a mathematical algorithm must be representative of the fluid–structure interaction that develops between the canopy and the surrounding flow. For the purpose of this research, the water column was divided into three flow regions: a bottom boundary layer, a canopy shear layer, and an internal canopy layer. The bottom boundary layer extends upwards from the bed to the point of maximum velocity between the bed and the suspended canopy. The canopy shear layer extends from the top of the bottom boundary layer some distance into the suspended canopy. Shear between flows in the canopy layer and beneath is the primary producer of turbulence in the canopy shear layer. In the internal canopy layer, turbulence is primarily generated by local mixing induced by the canopy elements. The different formulations used to include canopy effects are discussed in the following sub-sections.

2.3.1 *Constant drag coefficient model (CCDM) description*

The CCDM represents physical obstructions to flow by including an additional drag term in the momentum equation. In this formulation, the model incorporates the suspended canopy effect by using a bluff body, drag force equation:

$$F_D = \frac{aC_D\bar{u}\sqrt{\bar{u}^2 + \bar{v}^2 + \bar{w}^2}}{2} \tag{3}$$

where a denotes projected area of canopy per unit volume, C_D is the drag coefficient, and F_D is the drag per unit fluid mass. Incorporating this drag effect into the model, the governing equation of flow becomes (in the x-direction):

$$\begin{aligned}\frac{\partial(H\bar{u})}{\partial t} + \frac{\partial(H\bar{u}\bar{u})}{\partial x} + \frac{\partial(H\bar{v}\bar{u})}{\partial y} + \frac{\partial(\bar{w}\bar{u})}{\partial z} - fH\bar{v} \\ = -\frac{H\partial(p + g\eta)}{\partial x} + \left(\frac{\partial h}{\partial x} + z\frac{\partial H}{\partial x}\right)\frac{\partial p}{\partial z} \\ + \frac{\partial((\nu_v/H)(\partial\bar{u}/\partial z))}{\partial z} - F_D H\end{aligned} \tag{4}$$

where f is the Coriolis parameter, p is the pressure in excess of the reference density hydrostatic pressure, $\rho_0 gH(1-z)$, divided by the reference density, ρ_0. The final term on the right side, $F_D H$, is an extension to the original equations to represent canopy effects.

Specification of the drag coefficient is critical for the CCDM. Factors influencing the characterization of drag coefficient include flow conditions, canopy density and the shape of the canopy elements (Ghisalberti & Nepf, 2004). Laboratory investigations by Shimizu and Tsujimoto (1994) on flows through a vegetative canopy gave drag coefficients in the range of 1.0–1.5. Wu and Wang (2004) used laboratory studies of flow through a distributed array of emergent wooden dowels to verify a numerical model across a range of canopy densities. The authors reported optimum agreement between numerical and experimental results using drag coefficients of 0.8, 1.0, 1.8, and 3.0, corresponding to canopy densities of 0.04%, 0.2%, 0.6%, 2.5%, and 10% and Reynolds number ranging from 40 to 9600. O'Donncha et al. (2012) observed similar results when amending a depth-integrated numerical model to investigate the additional resistance created by aquaculture farms, with a drag coefficient of 1.8 yielding the best agreement with experimental data. These results demonstrate the wide range of possible values and the importance of experimental data to calibrate a model.

2.3.2 *Drag turbulence model (DTM) description*

The effects of canopy elements on turbulence production and dissipation have been widely discussed in the literature, particularly in relation to flows through vegetated canopies (Kang & Choi, 2006; Katul, Mahrt, Poggi, & Sanz, 2004; Naot et al., 1996; Neary, 2003; Poggi, Porporato, Ridolfi, Albertson, & Katul, 2004; Shimizu & Tsujimoto, 1994). The dominant length scale of turbulence is determined by the dimensions of the obstructing body (the canopy element), while turbulence intensity is augmented by the conversion of ambient mean kinetic energy to turbulent kinetic energy. (Nepf, 1999; Nepf, Sullivan, & Zavistoski, 1997). Two-equation turbulence closure models (such as the Mellor–Yamada scheme) are the simplest models that explicitly parameterize the multiple scales of vertical shear found in canopy environments (King et al., 2012).

As a first step in the development, we express the Mellor–Yamada turbulence model in terms of a generic length scale (GLS) model (Warner, Sherwood, Arango, & Signell, 2005).

The GLS approach is a two-equation model that takes advantage of similarities in a range of two-equation turbulence formulations (Umlauf & Burchard, 2003). The first equation in the GLS model is the standard equation of transport of turbulent kinetic energy k, while the second equation describes the transport of a generic parameter ψ, used to establish the turbulence length scale (l). The first equation is:

$$\frac{\partial k}{\partial t} + \bar{u}\frac{\partial k}{\partial x} + \bar{v}\frac{\partial k}{\partial y} + \bar{w}\frac{\partial k}{\partial z} = \frac{\partial k}{\partial z}\left(\frac{\nu_v}{\sigma_k}\frac{\partial k}{\partial z}\right) + P + B - \varepsilon \quad (5)$$

where k is turbulent kinetic energy (per unit mass), and σ_k is the turbulent Schmidt number for k. The terms P and B represent production by shear and buoyancy, respectively, as:

$$P = \nu_v\left[\left(\frac{\partial \bar{u}}{\partial z}\right)^2 + \left(\frac{\partial \bar{v}}{\partial z}\right)^2\right] \quad (6)$$

$$B = \nu_b\frac{g}{\rho_0}\frac{\partial \rho}{\partial z} \quad (7)$$

where ν_b refers to the turbulent diffusivity, ρ_0 is the reference density of the fluid, and ρ is the fluid density, that is a function of temperature and salinity. Dissipation rate, ε, is defined as:

$$\varepsilon = (c_\mu^0)^{3+p/n}k^{3/2+m/n}\psi^{-1/n} \quad (8)$$

where c_μ^0 is the stability coefficient based on experimental data, and p, m, and n are coefficients unique to each particular turbulence scheme. The second equation in the GLS model is:

$$\frac{\partial \psi}{\partial t} + u\frac{\partial \psi}{\partial x} + v\frac{\partial \psi}{\partial y} + w\frac{\partial \psi}{\partial z} = \frac{\partial}{\partial z}\left(\frac{\nu_v}{\sigma_\psi}\frac{\partial \psi}{\partial z}\right) + \frac{\psi}{k}(c_1P + c_3B - c_2\varepsilon F_{\text{wall}}) \quad (9)$$

where c_1, c_2 and c_3 are coefficients to be determined based on experimental observations, the parameter σ_ψ is the turbulence Schmidt number for ψ, and:

$$\psi = (c_\mu^0)^p k^m l^n \quad (10)$$

The parameters p, m, n, σ_k, σ_ψ, c_μ^0, c_1, c_2, c_3, and F_{wall} can be specified to recover exact formulations of the standard k-kl (Mellor–Yamada), k-ε or k-ω models (Warner et al., 2005). The specification of the equations in this manner facilitates comparison between turbulence models, while any theoretical or empirical developments to one model can be extended to others. The work of Shimizu and Tsujimoto (1994) and Neary (2003), on the k-ε and k-ω models respectively, serves as the basis for the amended scheme presented here. Adopting appropriate GLS parameters, the Mellor–Yamada turbulence scheme incorporating the additional canopy related turbulence terms is expressed as:

$$\frac{\partial k}{\partial t} + \bar{u}\frac{\partial k}{\partial x} + \bar{v}\frac{\partial k}{\partial y} + \bar{w}\frac{\partial k}{\partial z} = \frac{\partial}{\partial z}\left(\frac{\nu_v}{\sigma_k}\frac{\partial k}{\partial z}\right) + P + B - \varepsilon + C_{fk}F_D(\bar{u}+\bar{v}) \quad (11)$$

$$\frac{\partial kl}{\partial t} + \bar{u}\frac{\partial kl}{\partial x} + \bar{v}\frac{\partial kl}{\partial y} + \bar{w}\frac{\partial kl}{\partial z} = \frac{\partial}{\partial z}\left(\frac{\nu_v}{\sigma_l}\frac{\partial kl}{\partial z}\right) + l(c_1P + c_3B - c_2\varepsilon F_{wall} + C_{fl}F_D(\bar{u}+\bar{v})) \quad (12)$$

In these equations, the final term on the right is an extension to the original turbulence scheme to represent canopy drag-related turbulence production as expressed in Eq. (3), and C_{fk} and C_{fl} denote canopy turbulence weighting coefficients. These coefficients were fine-tuned as part of the model calibration process. Lopez and Garcia (2001) developed theoretical values for these weighting coefficients by reducing the three-dimensional k-ε equations to one dimension by averaging over space and time. Considering steady flow through an array of infinitely long cylinders, they demonstrated that C_{fk} and C_{fl} equal 1.0 and 1.33, respectively. However, the same study noted that experimental comparisons yielded measured values that were much lower, with improved agreement observed when prescribing values of zero rather than the theoretical coefficients.

2.3.3 *Vertically varying drag coefficient*

A large body of research exists to suggest that the drag force due to flow past a submerged cylinder is not uniform along its length. The free end of a cantilevered cylinder generates strong vortices near the tip that causes significant disturbances to the wake structure (Fox & West, 1993). The induced disturbances at the tip result in an increase in wake pressure, which leads to a reduction in drag compared to an infinitely long cylinder (Kawamura, Hiwada, Hibino, Mabuchi, & Kumada, 1984).

Dunn, Lopez, and Garcia (1996) investigated local drag coefficients within an array of rigid, submerged cylinders. Table 2 presents dimensional information on the range of canopy configurations considered. Their experiments demonstrated that drag along the length of the cylinders typically reached a maximum within the canopy, before diminishing towards a minimum at the tip of the cylinders. The best-fit drag coefficient profile reaches a maximum at a distance $h(z)/h_c = 0.38$ (where $h(z)$ represents distance from bed and h_c is the height of canopy), from the bed before decreasing, almost linearly, from a maximum of 1.3 to a value of 0.56 at the canopy interface. The magnitude of the bulk drag coefficient, C_{DA}, ranged from 1.02 to 1.42 across the various canopy densities (Table 2). Ghisalberti and Nepf (2004) observed similar trends in laboratory flume studies of flow within and above a simulated vegetated canopy. The profile of drag coefficient that provided best agreement with

measurements had a value of 0.45 at the bed, reached a maximum at a distance $h(z)/h_c = 0.76$ from the bed, and decreased to zero at the canopy tip. The magnitude of bulk drag coefficient C_{DA} ranged from 0.79 to 1.4, with the lower values corresponding to higher canopy densities. Model configurations developed based on the drag coefficient profile of Dunn et al. (1996) and Ghisalberti and Nepf (2004) will henceforth be referred to as DLGM and GNM, respectively.

The aforementioned experimental studies concerned submerged vegetation rather than a suspended canopy, and there are obvious discrepancies between the two systems. In particular, flows above a submerged canopy are subject to a free surface boundary condition, while flows beneath the suspended type are constrained by a solid boundary condition at the bed. Figure 1 presents both configurations, and highlights the contrasting effects of the free surface and bed in the submerged and suspended canopies respectively. However, as a preliminary step the suspended canopy was assumed to behave as an "inverted" submerged canopy. To compensate for the inherent differences between the submerged and suspended canopy types, the final stage of this study defined a modified drag profile with the coefficients tuned to provide best-fit agreement with the experimental data. This model is termed the EFDC aquaculture model (EAM). Figure 3 presents the three different vertical profiles of drag coefficient applied to the suspended canopy case.

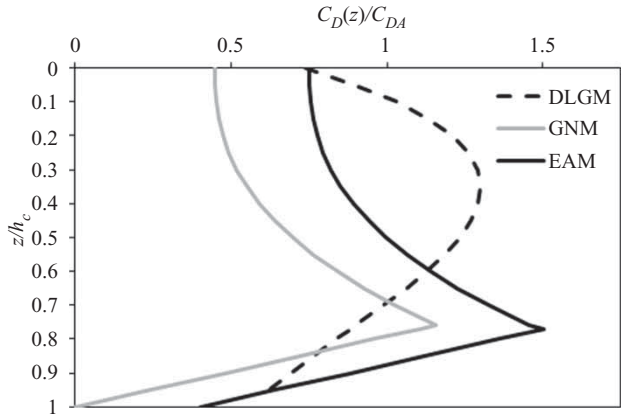

Figure 3 Computed profiles of vertical drag coefficient based on the works of Dunn et al. (1996) (DLGM), Ghisalberti and Nepf (2004) (GNM), and best-fit agreement with experimental data (EAM). The height of canopy is denoted by h_c, z is distance from free surface, C_{DA} is the bulk drag coefficient of an emergent array of cylinders, and $C_D(z)$ is the vertically varying drag coefficient

The drag coefficient profile adopted for the EAM model consists of a modified version of that proposed by Ghisalberti and Nepf (2004), with particular emphasis on the drag exerted at the canopy interface. Consequently, the profile of drag coefficient that provided best agreement with the experimental data reached a maximum value at a depth $h(z)/h_c = 0.76$ from the water surface, before decreasing to 0.4 at the canopy interface (Fig. 3). Considering the difficulties in obtaining exact agreement across all canopy densities, the approach focused on replicating flows from the higher density experimental runs (A1 and A2) with the remaining two experimental datasets used to assess the sensitivity of the model to canopy density. Hence, the selected drag profile is that which minimizes root mean square differences (RMSDs) between modelled and measured velocities for runs A1 and A2. The five model formulations and their distinguishing features are summarized in Table 3.

2.4 *Model set-up*

To preclude issues associated with scaling of experimental parameters to prototype scale (Hughes, 1993), model simulations adopted the same dimensional configurations as the experiments encompassing an area 6 m long by 0.6 m wide. A constant inflow (Table 1) was applied at the upstream boundary, and the water elevation specified at the downstream open boundary.

Table 2 Experimental configuration adopted by Dunn et al. (1996), Ghisalberti and Nepf (2004) and Plew (2011a)

Model	Array configuration (−)	a (m^{-1})	h_c/H (−)	Flume dimensions (m)
DLGM	Staggered rows	0.27–2.46	0.3–0.71	19.5 × 0.91 × 0.61
GNM	Randomly distributed	2.5–8	0.3	24 × 0.38 × 0.47
EAM	Aligned rows	0.48–1.9	0.5	6.0 × 0.6 × 0.2

Table 3 Description of methodologies used to represent canopy flow processes

Acronym	Name	Description of numerical representation
CCDM	Constant coefficient model	Additional drag term as discussed in Section 2.1 with original MY2.5 turbulence scheme
DTM	Drag and turbulence model	Drag term and amended turbulence scheme
DLGM	Dunn Lopez Garcia model	C_D (z) profile computed based on Dunn et al. (1996); amended MY2.5 turbulence scheme
GNM	Ghisalberti & Nepf model	C_D (z) profile computed based on Ghisalberti and Nepf (2004); amended MY2.5 turbulence scheme
EAM	EFDC aquaculture model	C_D (z) profile that provides best-fit agreement with measured data; amended MY2.5 turbulence scheme

All simulations adopt the amended momentum equations incorporating bluff body drag term F_D as presented in Eq. (3).

The horizontal grid spacing was chosen to ensure fully developed flow with no extraneous boundary effects within the domain. Based on model sensitivity studies a horizontal spacing of 0.1 m was adopted while a highly refined vertical grid of 0.005 m ensured adequate resolution of canopy shear layer processes. The horizontal grid size was significantly larger than the vertical as is common in ocean modelling studies (Chassignet & Verron, 2006). Accurate simulation of the vertical flow structure imposed by the suspended canopy effects drove the need for fine resolution in the vertical. The distribution of the canopy across the width of the domain meant that no comparable flow gradients developed in this direction and a coarser horizontal resolution sufficed.

The model equations are resolved using a combination of finite difference and finite volume techniques. The governing equations are horizontally discretized over boundary-fitted, orthogonal curvilinear coordinates where the model state variables are staggered on an Arakawa C-grid (Arakawa & Lamb, 1977). In the vertical direction, the equations are integrated over a cell layer. The numerical solution of the vertically discrete equations proceeds by splitting the external depth-integrated mode associated with external long surface gravity waves from the internal mode associated with vertical current structure. Hamrick (1992) provides further details on the numerical discretization and solution.

3 Results

3.1 *Constant coefficient drag model*

Results from the CCDM were compared to experimental data for all configurations. Figure 4 compares numerical output to experimental data from runs A1 and A3 while Table 4 presents RMSDs between modelled and measured data for all experiments. Figure 4a presents profiles of the numerically computed normalized streamwise velocity $\bar{u}/U_0$, where U_0 is the cross-sectional average velocity, while Fig. 4b presents normalized turbulent shear stress, defined as $\overline{u'w'}/U_0^2$. In general, the model approximates the flow profiles derived from the experimental data reasonably well. In particular the model replicates reduced flows within the canopy, increased current speed beneath, and large turbulence production at the canopy interface.

As discussed previously, accurate specification of the drag coefficient is the primary consideration for the CCDM. This parameter is considered part of model calibration and adjusted to provide best agreement with experimental data. Results demonstrate a dependency between drag coefficient and canopy density: a drag coefficient of 2.0 provided best agreement between numerical and experimental profiles for experimental set-up A1 (highest density of cylinders, Table 4), while a drag coefficient of 1.0 produced best-fit for dataset A4. The calibrated model fails to replicate certain features of the experimental flows, underestimating flow retardation at the bottom of the canopy and overestimating at the free surface. In addition, the model

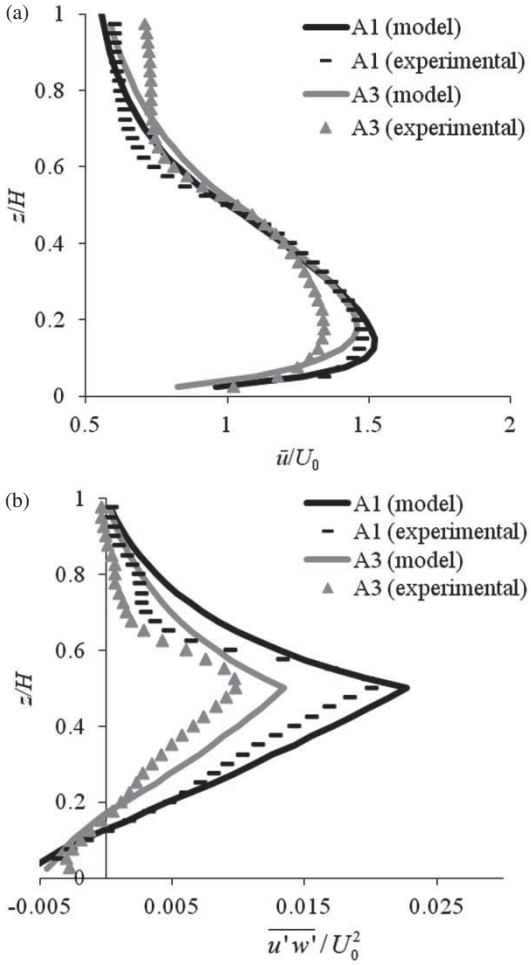

Figure 4 CCDM model results plotted against the experimental data for (a) normalized velocity and (b) turbulent shear stress variance of turbulence fluctuations. Canopy configurations A1 and A3 are presented

does not accurately track the experimental profile of turbulent shear stresses.

3.2 *Drag and turbulence model (DTM)*

The DTM extends the CCDM model further by amending the turbulence scheme to simulate canopy effects. Turbulence induced by the presence of the structure is represented via an additional production term in the turbulence closure equations. Calibration of the DTM involves parameterizing coefficients for both the momentum (as in the CCDM) and turbulence scheme equations. To permit comparisons with the CCDM, we use the same drag coefficient (2.0) for the momentum term while a value of 1.0 is prescribed for the drag coefficient in the turbulence production term (Eqs (11) and (12)). Calibration of the amended turbulence scheme is achieved by specifying appropriate canopy weighting coefficients to provide good agreement with experimental data. This study considers three cases: C_{fk} and C_{fl} equal to 0.0 making the DTM functionally equivalent to the CCDM; the theoretical values derived by Lopez and Garcia (2001) of C_{fk} and C_{fl} equal to 1.0 and 1.33 respectively; and universal values

Table 4 Root mean square differences computed between both model velocity and turbulent shear stresses, relative to experimental data

Experiment	5		A2		A3		A4	
Model	$\bar{u}$ (m s^{-1})	$\overline{u'w'}$ (m^2 s^{-2})	$\bar{u}$ (m s^{-1})	$\overline{u'w'}$ (m^2 s^{-2})	$\bar{u}$ (m s^{-1})	$\overline{u'w'}$ (m^2 s^{-2})	$\bar{u}$ (m s^{-1})	$\overline{u'w'}$ (m^2 s^{-2})
CCDM_1	0.078	0.558	0.072	0.675	0.069	0.679	0.065	1.33
CCDM_2	0.041	0.452	0.050	0.530	0.072	0.911	0.111	1.68
DTM	0.062	0.413	0.066	0.453	0.059	0.772	0.043	1.34
DLGM	0.056	0.665	0.078	0.784	0.112	1.174	0.163	1.34
GNM	0.051	0.582	0.047	0.601	0.048	0.826	0.077	1.67
EAM	0.043	0.495	0.045	0.516	0.058	0.761	0.093	1.39

The metrics are normalized by the mean of the experimental data for both velocity and turbulent shear stress. The first column presents the different model implementations, with further details given in Table 3. We present results for two separate parameterizations of the CCDM model, with prescribed drag coefficients of 1.0 and 2.0 represented by CCDM_1 and CCDM_2, respectively.

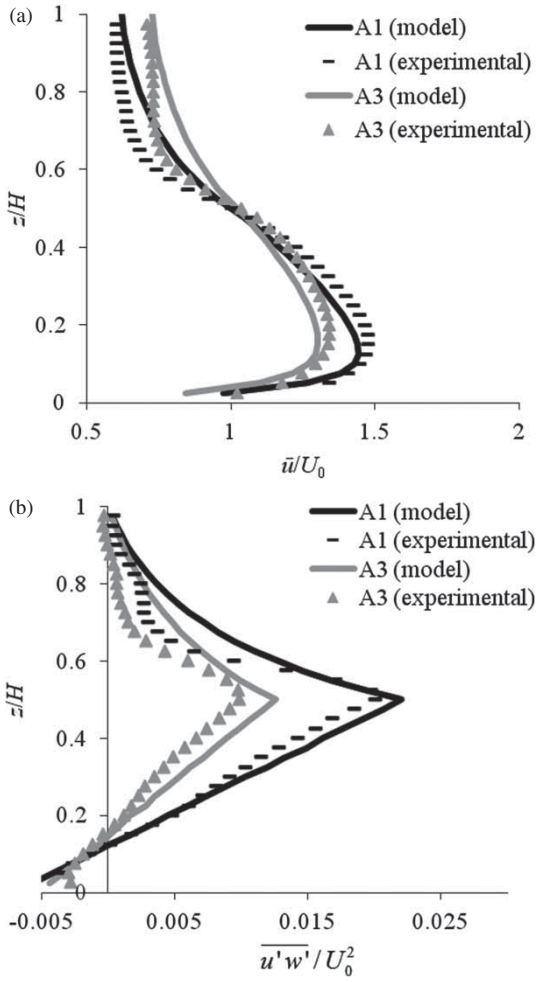

Figure 5 DTM model results plotted against the experimental data for (a) normalized velocity and (b) turbulent shear stress. Canopy configurations A1 and A3 are presented

from literature of C_{fk} and C_{fl} equal to 0.07 and 0.16 respectively (Lopez & Garcia, 2001; Neary, 2003; Shimizu & Tsujimoto, 1994).

Figure 5 presents the vertical velocity profile and turbulent shear stress predicted by the DTM parameterized with universal weighting coefficients (0.07 and 0.16). These coefficients provided closest agreement to the experimental data. Simulations using the larger weighting coefficients consistently overestimated turbulence stresses (see O'Donncha, 2012, p. 190). This is consistent with comparable research on submerged canopies in which values of weighting coefficients approaching zero produced better results than the larger, theoretical values (Lopez & Garcia, 2001; Neary, 2003). In general, the DTM outputs are closer to measured values of velocity and turbulent shear stresses across the different canopy densities than the CCDM. While the magnitude of velocity attenuation is similar to the CCDM, the velocity profiles are quite different. The DTM produces a more uniform profile within the canopy and better approximates velocities at the free surface, in particular for simulation A3. The amended vertical profile is a result of the additional turbulence production terms inducing greater momentum transfer between layers and thereby generating a more uniform flow profile (Nepf & Vivoni, 2000).

3.3 *Vertically varying drag coefficient*

This section presents numerical simulations incorporating a drag coefficient, $C_D(z)$, that varies in the vertical. Three different profiles, termed DLGM, GNM and EAM were investigated. Figure 3 presents the three different drag coefficient profiles whose derivation was presented in Section 2.3.

Figure 6 compares output from both DLGM and GNM model simulations, against experimental data for canopy configuration A1. Results demonstrate a number of shortcomings for both formulations. The DLGM overestimates velocity attenuation at the water surface and turbulent shear stress in the internal canopy layer. The GNM replicates measured data reasonably well but underestimates both velocity and turbulent shear stress at the canopy interface and water surface. A detailed analysis of these results led to the development of a refined drag coefficient varying along the length of the cylinder to improve agreement with observed data. The refined drag coefficient is an extension of the GNM drag profile. The refined profile amends the GNM drag profile by increasing drag at the top and bottom of the canopy to provide closest agreement to the measured data. In particular, analysis of results demonstrates that the GNM specification of zero drag at the tip of the canopy is unsuitable for this study.

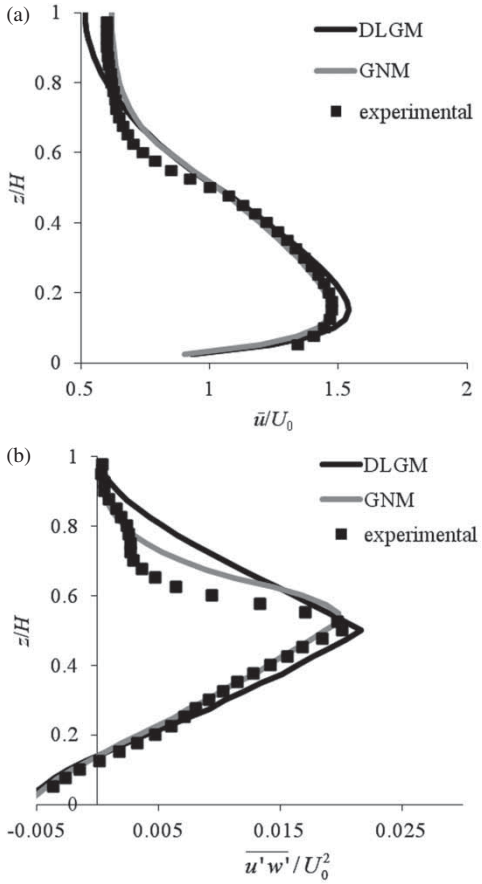

Figure 6 Comparison of DLGM and GNM model results compared to experimental data for canopy configuration A1. The figures present profiles of (a) mean velocity and (b) turbulent shear stress variance of turbulence fluctuations. An integrated bulk drag coefficient C_{DA} of 2.0 and 2.4 provided best-fit agreement for the DLGM and GNM respectively

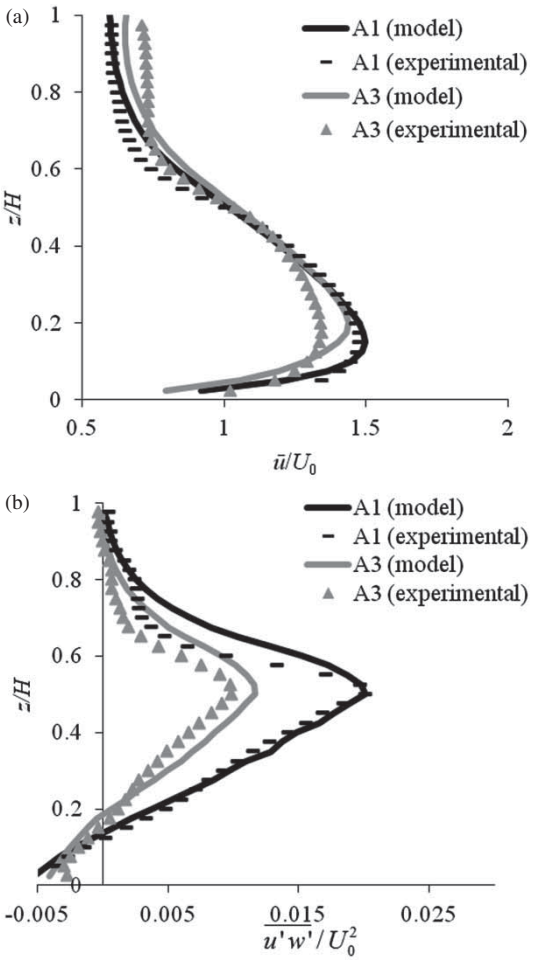

Figure 7 EAM model results plotted against the experimental data for (a) mean velocity and (b) turbulent shear stress variance of turbulence fluctuations. Canopy configurations A1 and A3 are presented

The EAM profile defines a drag coefficient of 0.4 at the canopy interface, increasing to a maximum at a distance $h(z)/h_c = 0.76$ from the water surface. Figure 3 presents the drag coefficient profile for the three separate implementations.

Figure 7 presents the velocity and turbulent shear stress profiles calculated using this drag profile. Comparisons show that the model performs well in simulating observed processes, particularly at the higher cylinder densities. The model accurately simulates both velocity profiles and turbulent stresses. In addition, the model reproduces the canopy shear layer and associated processes. Good agreement is obtained with measured values of turbulence, in both magnitude and structure. As discussed, model calibration focused on replicating measured flow processes for the higher density canopy configuration (i.e. A1 and A2). Results demonstrate that the parameterized model does not accurately capture flow processes for the lower canopy densities (i.e. A3 and A4). While the vertical profile of both velocity and turbulence shear stresses are replicated, the EAM overestimated the magnitude of both. This suggests that the magnitude of drag coefficient is excessive for the lower density canopies. The next section discusses these results and their implications.

4 Discussion

Table 4 presents RMSDs between modelled and measured data for the different model formulations. These metrics facilitate an assessment of the performance of each configuration and their ability to represent canopy flow processes. For convenience, this section focuses on an analysis of the different model implementations in order of increasing complexity: drag term in momentum equations (CCDM), drag and amended turbulence scheme (DTM), and finally drag with a vertically varying drag coefficient and amended turbulence scheme (DLGM, GNM and EAM).

Figure 4 demonstrates that the CCDM does not accurately replicate the rapid decrease in turbulent shear stress observed within the lower parts of the inner canopy. Instead, the model predicts a gradual and continuous reduction in shear stresses into and within the canopy. This suggests that the model is not accurately simulating the flow processes that develop within a suspended canopy. In particular, canopy shear layer processes are not well simulated. The exaggerated values of turbulent shear stress in the canopy transfer more momentum into the

upper canopy, resulting in velocity attenuation in the upper canopy greater than observed. Analysis of actual magnitudes of turbulence indicates that the CCDM over-predicts the turbulent shear stress at the interface and misrepresents the location of the maximum. The parameterized drag force is excessive at the bottom of the canopy and consequently the model overestimates the actual shear stresses imparted by the canopy at the interface. Another possibility is that the bottom boundary layer impedes the development of turbulence within the canopy. In flows over submerged canopies, Nepf and Vivoni (2000) observed that the free surface restricted the scale of the active turbulence at the top of the canopy when $H/h_c < 2.0$ (in this study $H/h_c = 2.0$). For a suspended canopy the no-slip boundary condition at the bed is expected to exacerbate the suppression of flow processes, relative to the free-surface boundary condition present in the submerged canopy case, for which the greatest amount of reference material exists (Nepf, Ghisalberti, White, & Murphy, 2007; Raupach & Thom, 1981). Plew (2011a) presents further details on the impact of the boundary beneath the canopy on the development of the mixing layer in the lower part of the canopy.

Analysing DTM results suggests that turbulence generated at the canopy scale does not significantly augment ambient turbulent stresses, with the greatest contribution developing due to the vertical flow gradient. In fact, results demonstrate a slight decrease in turbulence at the canopy interface for simulation A1, compared with CCDM output. However, the profiles of velocity are significantly affected, which has implications for the turbulent structure. It is apparent from Eqs (11) and (12) that, in addition to the turbulence transport terms on the left hand side of the equations, velocity shear, P, and buoyancy, B, are potentially important generators of turbulence. While in this study buoyancy is negligible, because the fluid in the flume is at a constant density, shear production is of major importance due to the vertical flow structure induced by the suspended canopy. The additional turbulence induced by the canopy term reduces the magnitude of velocity shear at the canopy interface due to increased momentum transfer between layers (Nepf & Vivoni, 2000). This reduction in shear velocity reduces the production of shear turbulent energy, and hence turbulence. Therefore, total canopy-induced turbulence becomes a combination of the reduced shear-generated turbulence and increased canopy layer turbulence simulated by the amended scheme. These results reassert that accurately representing the velocity profile is critical to reproducing the turbulence stresses.

A preliminary analysis of model output incorporating a drag coefficient varying in the vertical direction demonstrates improved simulation relative to observed flow conditions (Figs 6 and 7). The model better simulates the rapid attenuation of flow that develops at the bottom of the canopy together with a decrease in drag toward the free surface. The choice of vertical drag formulation is of importance; the direct application of a profile derived for a submerged canopy did not prove adequate for simulating suspended canopy processes. Results demonstrate that while the DLGM computes actual magnitudes of turbulent shear stress satisfactorily at the canopy interface, it did not reproduce the distribution of turbulent shear stress inside the canopy. As previously alluded to, the turbulent shear stress reduces quite rapidly within the experimental configuration; the model, on the other hand, predicts a near linear reduction from the canopy interface to the water surface. In this aspect, the DLGM model performed worse than the less sophisticated CCDM.

Of interest in this study was the location of maximum drag along the length of a cylinder. Dunn et al. (1996) determined the peak drag to be located at a distance $h(z)/h_c = 0.38$ from the bottom, while, conversely, Ghisalberti and Nepf (2004) observed drag to reach a maximum at a distance of 0.76. In this study, the profile proposed by Ghisalberti and Nepf (2004) provided better agreement with experimental data. A significant discrepancy with experimental data was the under-prediction of velocity attenuation and turbulent shear stress at the canopy interface. Extensive data exists on the effects of the free end of a cantilevered cylinder on flow, and the corresponding generation of coherent vortices and wake disturbances (Gambi, Nowell, & Jumars, 1990; Ghisalberti & Nepf, 2004; Raupach & Thom, 1981). GNM simulations predict that peak turbulent shear stress occurs within the canopy, rather than at the tip of the canopy as experimental results demonstrate. These points raise concern over the drag profile adopted for the GNM and in particular the specification of zero-drag at the tip of the canopy.

The implementation of a refined vertically varying drag coefficient along with an amended turbulence closure scheme provides closest agreement with measured values. In particular, the rapid attenuation of flows at the bottom of the canopy is closely approximated by the amended drag coefficient profile. The model accurately simulates both velocity profiles and turbulent structure, in addition to canopy shear layer processes across many of the canopy densities. However, discrepancies exist at lower canopy densities with both velocity and turbulence shear stress profiles suggesting that magnitude of drag coefficient is overestimated for experiments A3 and A4. RMSD values presented in Table 4 provide a measure of EAM model performance across all canopy densities.

Generally, EAM provides the best model simulation but there are aspects when other models perform better. The results illustrate that the EAM provides close approximations of measured flow processes across the different canopy densities. However, to provide a highly accurate representation, a drag coefficient that takes into account the effects of canopy density would be a useful extension. Traditionally this is done by tuning model parameters to individual case studies. As part of the research deriving from this study, the authors are developing a detailed relationship between drag coefficient and canopy density that will allow for a more universal model of canopy flow processes. By calibrating model drag coefficients against experimental flow data from a wide range of canopy densities, a drag coefficient specific to each density may be defined. It is expected that an explicit relationship between drag coefficient

and canopy density will permit a more precise model of canopy flows without the need for case-specific tuning of canopy drag terms. Further, the calibration of model drag coefficients against experimental data can be automated using parameter estimation models such as the parameter estimation (PEST) model (Doherty, 2010). PEST adjusts specified model parameters (here C_D, C_{fk}, and C_{fl}), until the fit between model outputs and measurements yields a minimized weighted least squares. This serves the dual purpose of making model calibration less tedious and also guaranteeing best fit against experimental data.

In the approach presented in this paper, the canopy drag force is assumed to be a quadratic function of velocity. This is appropriate for rigid or semi-rigid objects, such as the circular cylinders used in the laboratory experiments, and shellfish farms (Plew, Enright, Nokes, & Dumas, 2009). Highly flexible structures may be more appropriately modelled using the Vogel exponent approach, where the velocity exponent of 2 for the rigid equivalent is reduced by the value of the Vogel exponent (Barois & De Langre, 2013; Fathi-Maghadam & Kouwen, 1997), and the conservation equations are modified appropriately. Flow-induced reconfiguration of the flexible canopy element also reduces flow resistance through two mechanisms. First, reconfiguration reduces the frontal area of the impeding body and, second, the reconfigured shape tends to be more streamlined (Nepf, 2012). In addition, in locations exposed to high wave energy, the flexibility of the canopy elements and turbulence generated by wave motion may also have an effect on turbulence and consequently mean flow distributions.

5 Conclusions

This study focused on numerical simulations of steady flow through a suspended canopy. Both the experiments and models were set up such that flow diversion is predominantly under, rather than around, the canopy (i.e. the canopy spans the width of the flume). Field studies of suspended canopies suggest that this is not always appropriate because there is significant horizontal diversion of flow around canopies that do not span the width of the flow system (Boyd & Heasman, 1998). Density stratification may also affect canopy flow processes by inhibiting vertical diversion and favouring instead a horizontal diversion (Plew et al., 2005). Further laboratory experiments investigating flow diversions under and around suspended canopies could address many of these issues. In addition, a comprehensive field monitoring programme would provide insight into the universality of the model and, in particular, the viability of the coefficients (C_D, C_{fk}, and C_{fl}) adopted here for real-world scenarios. However, the complexity of stratified flows through or around canopies makes detailed laboratory studies challenging and field studies costly and laborious. Considering these issues, numerical modelling is a vital tool for supplementing and expanding our understanding of the impacts of canopy-like structures on environmental flow processes.

This paper presents an amended three-dimensional model to simulate canopy flow processes. Results compare performance of the model against data from rigid cylinder arrays under suspended canopy conditions. Five different model implementations were investigated, namely: a constant drag coefficient model (CCDM) representing form drag imparted by the suspended canopy; a drag turbulence model (DTM) that includes a constant drag coefficient and amended turbulence scheme; and three separate formulations involving drag coefficient profiles varying in the vertical. Results show that the most accurate simulation of the canopy flow was obtained using a vertically varying drag coefficient, along with a two-equation turbulence closure scheme, which included additional turbulent production and dissipation terms. The amended model accurately reproduced observed flow structure, including attenuated flows within the canopy, shear layer flows, and accelerated free-stream flows beneath the canopy. The model has potential for widespread application to canopy flow investigations, combining a widely used hydro-environmental model and parameterized canopy effects to permit comprehensive assessment of circulation patterns at the bay scale.

Funding

Elements of this research were supported by the EnergyMARE and MAREN2 projects which were part-funded by the European Regional Development Fund (ERDF) through the Atlantic Area Transnational Programme (INTERREG IV). The authors are grateful to Bord Iascaigh Mhara (BIM) for financial support of this work in the framework of project "UISCE: Understanding Irish Shellfish Culture Environments".

Notation

a	=	projected area per unit volume (m^{-1})
B	=	turbulence production by buoyancy ($m^2\ s^{-3}$)
c_1, c_2, c_3	=	turbulence model empirical constants (–)
C_D	=	drag coefficient (–)
$C_D(z)$	=	vertically varying drag coefficient (–)
C_{DA}	=	integrated bulk drag coefficient within canopy (–)
C_{fk}, C_{fl}	=	canopy turbulence weighting coefficients (–)
f	=	Coriolis parameter (s^{-1})
F_D	=	drag force per unit fluid mass ($m\ s^{-2}$)
F_{wall}	=	turbulence model empirical constant (–)
g	=	gravity acceleration ($m\ s^{-2}$)
h	=	depth below datum (m)
h_c	=	height of canopy (m)
h_g	=	gap above or beneath canopy (m)
H	=	total water depth (m)
k	=	turbulence kinetic energy ($m^2\ s^{-2}$)
l	=	turbulence length scale (m)
L_x	=	streamwise spacing between cylinders (m)
L_y	=	cross-stream spacing between cylinders (m)

P = turbulence production by shear ($m^2\ s^{-3}$)
p = physical pressure in excess of the reference density hydrostatic pressure (Pa)
Q = flow rate ($m^3\ s^{-1}$)
U_0 = ambient upstream flow speed ($m\ s^{-1}$)
u, v, w = velocity components in the x, y and z directions, respectively ($m\ s^{-1}$)
u', v', w' = fluctuating components of velocity in the x, y and z directions, respectively ($m\ s^{-1}$)
$\bar{u}, \bar{v}, \bar{w}$ = mean components of velocity in the x, y and z directions, respectively ($m\ s^{-1}$)
$\overline{u'w'}$ = primary turbulent shear stress ($m^2\ s^{-2}$)
z^* = original physical vertical coordinates (m)
z = sigma vertical coordinates (–)
σ_k, σ_l = turbulence model empirical constants (–)
η = free surface displacement above or below datum (m)
ρ = density ($kg\ m^{-3}$)
ρ_0 = reference density ($kg\ m^{-3}$)
ν_v = turbulent viscosity ($m^2\ s^{-1}$)
ν_b = turbulent diffusivity ($m^2\ s^{-1}$)

References

Arakawa, A., & Lamb, V. R. (1977). Computational design of the basic dynamical processes of the UCLA general circulation model. *Methods in Computational Physics*, *17*, 173–265.

Barois, T., & De Langre, E. (2013). Flexible body with drag independent of the flow velocity. *Journal of Fluid Mechanics*, *735*, R2.1–R2.9.

Blanco, J., Zapata, M., & Morono, A. (1994). Some aspects of the water flow through mussel rafts. *Scientia Marina*, *60*(2–3), 275–282.

Boyd, A. J., & Heasman, K. G. (1998). Shellfish mariculture in the Benguela System: Water flow patterns within a mussel farm in Saldanha Bay, South Africa. *Journal of Shellfish Research*, *17*, 25–32.

Chassignet, E. P., & Verron, J. (2006). *Ocean weather forecasting: An integrated view of oceanography*. Dordrecht: Springer.

Doherty, J. (2010). *Model-independent parameter estimation* (user manual). Watermark Numerical Computing. Retrieved from http://www2.epa.gov/sites/production/files/documents/PESTMAN.PDF

Dunn, C., Lopez, F., & Garcia, M. (1996). *Mean flow and turbulence in a laboratory channel with simulated vegetation*. (Hydraulic Engineering Series no. 51). Champaign, IL: Department of Civil Engineering, University of Illinois at Urbana-Champaign.

Fathi-Maghadam, M., & Kouwen, N. (1997). Nonrigid, Nonsubmerged, Vegetative Roughness on Floodplains. *Journal of Hydraulic Engineering*, *123*(1), 51–57. http://doi.org/10.1061/(ASCE)0733-9429(1997)123:1(51)

Fischer-Antze, T., Stoesser, T., Bates, P., & Olsen, N. R. B. (2001). 3D numerical modelling of open-channel flow with submerged vegetation. *Journal of Hydraulic Research*, *39*(3), 303–310. http://doi.org/10.1080/00221680109499833

Fox, T. A., & West, G. S. (1993). Fluid-induced loading of cantilevered circular cylinders in a low-turbulence uniform flow. Part 2: Fluctuationg loads on a cantilever of aspect ratio 30. *Journal of Fluids and Structures*, *7*(1), 15–28. http://doi.org/10.1006/jfls.1993.1002

Galperin, B., Kantha, L. H., Hassid, S., & Rosati, A. (1988). A quasi-equilibrium turbulent energy model for geophysical flows. *Journal of the Atmospheric Sciences*, *45*, 55–62. http://doi.org/10.1175/1520-0469(1988)045 < 0055:AQETEM > 2.0.CO;2

Gambi, M. C., Nowell, A. R. M., & Jumars, P. A. (1990). Flume observations on flow dynamics in Zostera marina (eelgrass) beds. *Marine Ecology Progress Series*, *61*, 159–169. http://doi.org/10.3354/meps061159

Gao, G., Falconer, R. A., & Lin, B. (2011). Modelling open channel flows with vegetation using a three-dimensional model. *Journal of Water Resource and Protection*, *3*, 114–119.

Ghisalberti, M., & Nepf, H. (2005). Mass transport in vegetated shear flows. *Environmental Fluid Mechanics*, *5*(6), 527–551.

Ghisalberti, M., & Nepf, H. M. (2002). Mixing layers and coherent structures in vegetated aquatic flows. *Journal of Geophysical Research*, *107*(C2), 1–11. http://doi.org/10.1029/2001JC000871

Ghisalberti, M., & Nepf, H. M. (2004). The limited growth of vegetated shear layers. *Water Resources Research*, *40*, 1–12. http://doi.org/10.1029/2003WR002776

Grant, J., & Bacher, C. (2001). A numerical model of flow modification induced by suspended aquaculture in a Chinese bay. *Canadian Journal of Fisheries and Aquatic Sciences*, *58*, 1003–1011. http://doi.org/10.1139/cjfas-58-5-1003

Hamrick, J. M. (1992). *A three-dimensional environmental fluid dynamics computer code: Theoretical and computational aspects* (Special Report in Applied Marine Science and Ocean Engineering). Virginia Institute of Marine Science, College of William and Mary.

Hartstein, N. D., & Stevens, C. L. (2005). Deposition beneath long-line mussel farms. *Aquacultural Engineering*, *33*(3), 192–213. http://doi.org/10.1016/j.aquaeng.2005.01.002

Hughes, S. A. (1993). *Physical model and laboratory techniques in coastal engineering* (Vol. *7*). Singapore: World Scientific Publishing.

Ji, Z.-G. (2008). *Hydrodynamics and water quality: Modeling rivers, lakes, and estuaries*. Hoboken, NJ: John Wiley & Sons.

Kang, H., & Choi, S.-U. (2006). Turbulence modeling of compound open-channel flows with and without vegetation on the floodplain using the Reynolds stress model. *Advances in Water Resources*, *29*(11), 1650–1664. http://doi.org/10.1016/j.advwatres.2005.12.004

Katul, G. G., Mahrt, L., Poggi, D., & Sanz, C. (2004). One- and two-equation models for canopy turbulence. *Boundary Layer Meteorology*, *113*, 81–109. http://doi.org/10.1023/B:BOUN.0000037333.48760.e5

Kawamura, T., Hiwada, M., Hibino, T., Mabuchi, I., & Kumada, M. (1984). Flow around a finite circular cylinder on a flat plate: Cylinder height greater than turbulent boundary layer thickness. *Bulletin of JSME*, *27*(232), 2142–2151. http://doi.org/10.1299/jsme1958.27.2142

King, A. T., Tinoco, R. O., & Cowen, E. A. (2012). A *k-ε* turbulence model based on the scales of vertical shear and stem wakes valid for emergent and submerged vegetated flows. *Journal of Fluid Mechanics*, *701*, 1–39. http://doi.org/10.1017/jfm.2012.113

King, J., & Tryfonas, T. (2009). Tidal stream power technology – State of the art. In OCEANS 2009 – EUROPE (pp. 1–8). http://doi.org/10.1109/OCEANSE.2009.5278329

Lenihan, H. S., Peterson, C. H., & Allen, J. M. (1996). Does flow speed also have a direct effect on growth of active-suspension feeders: An experimental test on oysters. *Limnology and Oceanography*, *41*(6), 1359–1366. http://doi.org/10.4319/lo.1996.41.6.1359

Lopez, F., & Garcia, M. H. (2001). Mean flow and turbulence structure of open-channel flow through non-emergent vegetation. *Journal of Hydraulic Engineering*, *127*(5), 392–402. http://doi.org/10.1061/(ASCE)0733-9429(2001)127:5(392)

McKindsey, C. W., Thetmeyer, H., Landry, T., & Silvert, W. (2006). Review of recent carrying capacity models for bivalve culture and recommendations for research and management. *Aquaculture*, *261*(2), 451–462. http://doi.org/10.1016/j.aquaculture.2006.06.044

Mellor, G. L., & Yamada, T. (1974). A hierarchy of turbulence closure models for planetary boundary layers. *Journal of the Atmospheric Sciences*, *31*(1), 1791–1806. http://doi.org/10.1175/1520-0469(1974)031 < 1791:AHOTCM > 2.0.CO;2

Naot, D., Nezu, I., & Nakagawa, H. (1996). Hydrodynamic behaviour of partly vegetated open channels. *Journal of Hydraulic Engineering*, *122*(11), 625–633. http://dx.doi.org/10.1061/(ASCE)0733-9429(1996)122:11(625)

Neary, V. S. (2003). Numerical solution of fully developed flow with vegetative resistance. *Journal of Engineering Mechanics*, *129*(5), 558–563. http://doi.org/10.1061/(ASCE)0733-9399(2003)129:5(558)

Neill, S. P., Litt, E. J., Couch, S. J., & Davies, A. G. (2009). The impact of tidal stream turbines on large-scale sediment dynamics. *Renewable Energy*, *34*(12), 2803–2812. http://doi.org/10.1016/j.renene.2009.06.015

Nepf, H. M. (1999). Drag, turbulence and diffusion in flow through emergent vegetation. *Water Resources Research*, *35*(2), 479–489. http://doi.org/10.1029/1998WR900069

Nepf, H. M. (2012). Hydrodynamics of vegetated channels. *Journal of Hydraulic Research*, *50*(3), 262–279. http://doi.org/10.1080/00221686.2012.696559

Nepf, H. M., Ghisalberti, M., White, B., & Murphy, E. (2007). Retention time and dispersion associated with submerged aquatic canopies. *Water Resources Research*, *43*, 10. http://doi.org/10.1029/2006WR005362

Nepf, H. M., Sullivan, J. A., & Zavistoski, R. A. (1997). A model for diffusion within emergent vegetation. *Limnology and Oceanography*, *42*(8), 1735–1745. http://doi.org/10.4319/lo.1997.42.8.1735

Nepf, H. M., & Vivoni, E. R. (2000). Flow structure in depth-limited, vegetated flow. *Journal of Geophysical Research*, *105*(C12), 28547–28557. http://doi.org/10.1029/2000JC900145

O'Donncha, F. (2012). *Physical and numerical modelling of impeded tidal flows: Effects of aquaculture structures on hydrodynamics and material transport* (Ph.D). National University of Ireland, Galway, Galway.

O'Donncha, F., Hartnett, M., & Nash, S. (2012). Physical and numerical investigation of the hydrodynamic implications of aquaculture farms. *Aquacultural Engineering*. http://doi.org/10.1016/j.aquaeng.2012.07.006

Phillips, N. A. (1957). A coordinate system having some special advantages for numerical forecasting. *Journal of Meteorology*, *14*, 184–185. http://doi.org/10.1175/1520-0469(1957)014 < 0184:ACSHSS > 2.0.CO;2

Plew, D. R. (2011a). A depth-averaged drag coefficient for modelling flow through suspended canopies. *Journal of Hydraulic Engineering*, *137*, 234–247. http://doi.org/10.1061/(ASCE)HY.1943-7900.0000300

Plew, D. R. (2011b). Shellfish farm-induced changes to tidal circulation in an embayment, and impications for seston depletion. *Aquaculture Environment Interactions*, *1*, 201–214. http://doi.org/10.3354/aei00020

Plew, D. R., Enright, M. P., Nokes, R. I., & Dumas, J. K. (2009). Effect of mussel bio-pumping on the drag on and flow around a mussel crop rope. *Aquacultural Engineering*, *40*(2), 55–61. http://doi.org/10.1016/j.aquaeng.2008.12.003

Plew, D. R., Stevens, C. L., Spigel, R. H., & Hartstein, N. D. (2005). Hydrodynamic implications of large offshore mussel farms. *IEEE Journal of Oceanic Engineering*, *30*(1), 95–108. http://doi.org/10.1109/JOE.2004.841387

Poggi, D., Porporato, A., Ridolfi, L., Albertson, J. D., & Katul, G. G. (2004). The effect of vegetation density on canopy sub-layer turbulence. *Boundary-Layer Meteorology*, *111*(3), 565–587. http://doi.org/10.1023/B:BOUN.0000016576.05621.73

Raupach, M. R., & Thom, A. S. (1981). Turbulence in and above plant canopies. *Annual Review of Fluid Mechanics*, *13*(1), 97–129. http://doi.org/10.1146/annurev.fl.13.010181.000525

Rodi, W. (1993). *Turbulence models and their application in hydraulics: A state-of-the art review* (3rd ed.). Rotterdam, Netherlands; Broofield, Vermont: International Association for Hydraulic Research.

Shapiro, G. I. (2010). Effect of tidal stream power generation on the region-wide circulation in a shallow sea. *Ocean Science*

Discussions, *7*(5), 1785–1810. http://doi.org/10.5194/osd-7-1785-2010

Shi, J., Wei, H., Zhao, L., Yuan, Y., Fang, J., & Zhang, J. (2011). A physical–biological coupled aquaculture model for a suspended aquaculture area of China. *Aquaculture*, *318*(3–4), 412–424. http://doi.org/10.1016/j.aquaculture.2011.05.048

Shimizu, Y., & Tsujimoto, T. (1994). Numerical analysis of turbulent open-channel flow over a vegetation layer using a k-e turbulence model. *Journal of Hydroscience and Hydraulic Engineering*, *11*(2), 57–67.

Umlauf, L., & Burchard, H. (2003). A generic length-scale equation for geophysical turbulence models. *Journal of Marine Research*, *61*(2), 235–265. http://doi.org/10.1357/002224003322005087

Venayagamoorthy, S. K., Fringer, O. B., Koseff, J. R., Chiu, A., & Naylor, R. L. (2011). Numerical modelling of aquaculture dissolved waste transport in a coastal embayment. *Environmental Fluid Mechanics*, *11*, 329–352. http://doi.org/10.1007/s10652-011-9209-0

Warner, J. C., Sherwood, C. R., Arango, H. G., & Signell, R. P. (2005). Performance of four turbulence closure models implemented using a generic length scale method. *Ocean Modelling*, *8*(1–2), 81–113. http://doi.org/10.1016/j.ocemod.2003.12.003

Wilson, C., Stoesser, T., & Bates, P. D. (2005). Modelling of open channel flow through vegetation. *Computational Fluid Dynamics: Applications in Environmental Hydraulics*, 395–428. http://doi.org/10.1002/0470015195.ch15

Wu, W., & Wang, S. S. Y. (2004). A depth-averaged two-dimensional numerical model of flow and sediment transport in open channels with vegetation. In S. J. Bennett & A. Simon (Eds.), *Riparian vegetation and fluvial geomorphology*. (pp. 253–265). Washington, DC: American Geophysical Union.